www.czasopisma.pan.pl PAN www.journals.pan.pl

ARCHIVES of FOUNDRY ENGINEERING

DE GRUYTER OPEN

DOI: 10.1515/afe-2017-0109

ISSN (2299-2944)
Volume 17
Issue 3/2017

Published quarterly as the organ of the Foundry Commission of the Polish Academy of Sciences

155 – 162

Phase Field Study of Microstructure Evolution in Eutectoid Phase Transformation – I Nucleation

Dongqiao Zhang, Yajun Yin, Jianxin Zhou *, Zhixin Tu
State Key Laboratory of Materials Processing and Die & Mould Technology,
Huazhong University of Science and Technology, Wuhan, 430074,China
* Corresponding author. E-mail address: zhoujianxin@hust.edu.cn

Received 01.03.2017; accepted in revised form 22.05.2017

Abstract

Eutectoid growth, as the important reaction mechanism of the carbon steel heat treatment, is the basis to control the microstructure and performance. At present, most studies have focused on lamellar growth, and did not consider the nucleation process. Mainly due to the nucleation theory is inconclusive, a lot of research can support their own theory in a certain range. Based on the existing nucleation theory, this paper proposes a cooperative nucleation model to simulate the nucleation process of eutectoid growth. In order to ensure that the nucleation process is more suitable to the theoretical results, different correction methods were used to amend the model respectively. The results of numerical simulation show that when the model is unmodified, the lateral growth of single phase is faster than that of longitudinal growth, so the morphology is oval. Then, the effects of diffusion correction, mobility correction and ledges nucleation mechanism correction on the morphology of nucleation and the nucleation rate were studied respectively. It was found that the introduction of boundary diffusion and the nucleation mechanism of the ledges could lead to a more realistic pearlite.

Keywords: Eutectoid, Nucleation model, Numerical simulation, Phase field

1. Introduction

At this stage, the nucleation model is mainly focused on the transformation process from one phase to another phase, such as the solid phase nucleated in the liquid phase, ferrite nucleated in austenite. The model can be divided into two types, one is the seed density model, that is based on the theory of uniform nucleation, The position of nucleus is given at random, and the particle radius distribution function gives the particle radius, then according to the free energy to determine whether the nucleation of particles. Another is seed undercooling model, that is, the nucleation is judged according to whether or not the degree of undercooling exceeds the critical nucleation degree of undercooling. For example, in 2006, Su Yanqing et al. [1] simulated the peritectic microstructure evolution during directional solidification. The nucleation criterion is that the solute component in the front of a phase growth interface reaches the critical component of the second phase. In 2011, Wu Mengwu et al. [2] simulated the binary regular eutectic growth using the cellular automaton method. The nucleation, bifurcation, annihilation and amalgamation were reconstructed according to the curvature and critical concentration state. In 2011, Liu Zongchang et al. carried out an experimental study on the nucleation of bainitic, and calculated the critical size and nucleation power of the nuclei, and provided the above two nucleation mechanisms [3]. In 2012, Wang Yonbiao et al. simulated the effect of interfacial effect on nucleation of grains.

The nucleation model was not proposed in this process, but it should be described as homogeneous nucleation theory [4]. In 2011 V.G.Vaks et al. studied nucleation and growth process of the eutectoid steel, the critical concentration value was obtained according to the relationship between the model and the concentration. The nucleus would be appeared when the concentration is higher than the critical value, the mechanism belongs to the critical undercooling model because the critical concentration value can be converted to the critical degree of undercooling [5]. The formation, nucleation and growth kinetics of ferrite in low carbon high strength steels were studied by Cheng Lin [6] in 2013, and the nucleation mechanism was described based on the experimental results. The nucleation model in this paper based on the theory, combined with three correction methods, the nucleation behavior of the cooperative growth mechanism was analyzed.

2. Mathematical model

2.1. Multi-phase field model

In this paper, the Ingo's model is adopted for multi-phase field. The total free energy function is composed of interfacial energy density, chemical energy density and other energy density. The phase field equation [7], the concentration field equation [8] and the stress-strain field equation [8] can be obtained after a series of derivation.

$$\phi_\alpha = \frac{1}{N}\sum_{\beta=1}^{N}\dot{\psi}_{\alpha\beta}$$

$$\dot{\psi}_{\alpha\beta} \dots_{\alpha\beta}\left\{\left[\sigma_{\alpha\beta}\left(I_\alpha - I_\beta\right) + \sum_{\gamma-1,\gamma\neq\alpha,\gamma\neq\beta}^{N}\left(\sigma_{\beta\gamma}-\sigma_{\alpha\gamma}\right)I_\gamma\right] + \frac{\pi^2}{4\eta}\Delta \dots_{\alpha\beta}\right\} \quad (1)$$

$$I_\alpha = \left\{\nabla^2\phi_\alpha + \frac{\pi^2}{\eta^2}\phi_\alpha\right\}$$

$$\dot{c} \dots \sum_{\alpha=1}^{N} \dots_\alpha\left(D_\alpha\nabla^i c_\alpha - \nabla^i M_\alpha\left(\varepsilon_\alpha^1\right)^{kl} s^{kl}\right) \quad (2)$$

$$0^i = \nabla^j \sum_{\alpha=1}^{N}\phi_\alpha C^{ijkl}\left(\varepsilon_\alpha - \left(\varepsilon_\alpha^0\right)^{kl} - c_\alpha\left(\varepsilon_\alpha^1\right)^{kl}\right) \quad (3)$$

Where ϕ_α, ϕ_β is the phase field of α, β or different orientation grain of the same phase. Where η is interface width. $\sigma_{\alpha\beta}$ is the interface energy between α and β. $\dot{\psi}_{\alpha\beta}$ is the interfacial field of phase α and β. $\mu_{\alpha\beta}$ is the interface mobility between α and β. N is the number of phases, respectively. c_α is the concentration of phase α, $(\varepsilon_\alpha^1)^{kl}$ is the first order tensor of total strain of phase $(\varepsilon_\alpha^0)^{kl}$ is the zero-order tensor of total strain of phase α. s^{kl} is the stress tensor, ε_α is strain of phase α, C_α^{ijkl} is the effective elasticity matrix. D_α is diffusion coefficient of phase α. M_α is chemical mobility of phase α. The paper mainly uses phase field model and concentration field model.

Phase field and concentration field are discretized by finite difference method, C language is used to encode, and the boundary of the simulated area is treated by adiabatic boundary condition.

2.2. Nucleation model

The nucleation process of pearlite consists of two aspects, one is how to determine the location of nucleation and the other is the realization of nucleation growth. Here, the nucleation growth is different from the subsequent growth model.

(1) Nucleation sites

The undercooling model can determine the nucleation sites well. When the degree of undercooling is lower than the critical undercooling, the position is set as the nucleation point. Since there are two phases in the pearlite nucleation process, it is necessary to judge the nucleation of the two phases separately. Due to the influence of the constitutional supercooling, the theoretical transition temperature will change when the actual concentration changes. Assuming that the GS, GP and ES lines in the Fe-C phase diagram are straight lines(shown in Fig. 1), the relationship between the composition and theoretical transition temperature can be obtained, as shown in Equations (5)and (6).

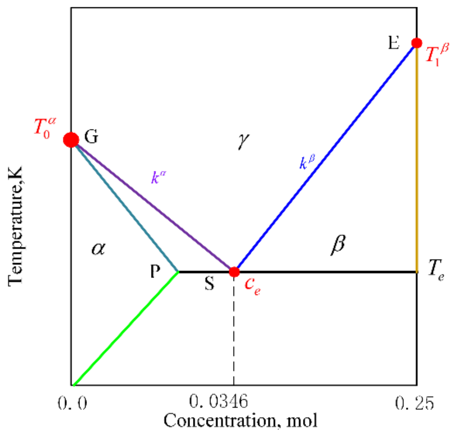

Fig. 1. Fe-C phase diagram

$$\Delta T = T^i - T_t^i \quad (1)$$

$$T_0^\alpha + k^\alpha \cdot C^\alpha = T^\alpha \quad (2)$$

$$T_1^\beta + k^\beta \cdot \left(C^\beta - 0.25\right) = T^\beta \quad (3)$$

Where ΔT is undercooling. T^i ($i=\alpha,\beta$) is the theoretical transition temperature. T_t^i ($i=\alpha,\beta$) is the actual temperature of phase i at time t. T_0^α is the melting point of pure iron. T_1^β is the melting point of cementite, corresponding to the theoretical transition temperature of 0.25 carbon mole fraction in the phase diagram. T^α is the temperature on line GS, T^β is the temperature on line ES, k^α is the slope of phase α, k^β is the slope of phase β, such as GS or

SE. C^{α} is the concentration of phase α, C^{β} is the concentration of phase β.
T_0^{α}, T_1^{β} and k^{α}, k^{β} are constants for Fe-C phase diagram, so ΔT changes with C^i ($i=\alpha,\beta$) when it is isothermal transition. So the nucleation position criterion equation (7) can be equivalent to equation (8).

$$\Delta T_{nucleation} > \Delta T_{critical} \tag{4}$$

$$\begin{aligned} C_{nucleation} > C_{critical} \quad k^i < 0 \\ C_{nucleation} < C_{critical} \quad k^i > 0 \end{aligned} \tag{5}$$

(2) Growth of the nuclei
When determining the nucleation sites, the nucleus begins to grow. Combined with the free energy density function, nucleus growth is essentially due to the driving force is greater than the surface energy. When the nucleus is too small, the surface energy is greater than the driving force, it is difficult to ensure that the nucleus can growth. So a critical volume value $V_{critical}^i$ can be given, when the nucleus volume is greater than the critical volume, the driving force term is greater than surface energy term. (Here the phase field equation is divided into two parts, namely the surface energy term and the driving force term, the surface energy is $\sigma_{\alpha\beta}\left(I_{\alpha}-I_{\beta}\right)+\sum_{\gamma=1,\gamma\neq\alpha,\gamma\neq\beta}^{N}\left(\sigma_{\beta\gamma}-\sigma_{\alpha\gamma}\right)I_{\gamma}$, and the driving force is $\frac{\pi^2}{4\eta}\Delta\tilde{\xi}_{-r}$. But when the nucleus volume is less than the critical volume, the surface energy term can be reduced to a certain value to meet the driving force term is greater than the surface energy term. That is, the original surface energy term can be multiplied by a scaling factor "*Scale*". At the same time, in order to ensure the stability of the numerical solution and avoid the problem that the radius of the nucleation point is smaller than the interface thickness [9], it is necessary to set the critical volume. Both of them must be satisfied at the same time. The scaling factor "*Scale*" is calculated as shown in **Błąd! Nie można odnaleźć źródła odwołania.**. V^i is the volume of phase *i*. The value of critical volume $V_{critical}^i$ is equal to $\pi\cdot\frac{width}{2}\cdot\frac{width+1}{2}$, the "*width*" is the number of interface grids.

$$Scale = \frac{V^i}{V_{critical}^i} \tag{9}$$

3. Nucleation mechanism and condition parameter setting

In this paper, we discuss the effect of nucleation on the growth of pearlite. Based on lamellar growth theory that a phase cling to another phase for growing, the simulation analysis is carried out from the simple volume diffusion mechanism, the boundary diffusion mechanism and the velocity control diffusion mechanism. Here, it is assumed that one of the phases in the eutectoid phase is precipitated first, then the other phase is precipitated. Therefore, there are two precipitation modes: first precipitation of ferrite and first precipitation of cementite. The nucleation mechanism is shown as follow. The first precipitate phase nucleated at the boundary. With the growing of nucleus, the second phase begins to nucleate when the neighbor region satisfies the nucleation condition of the second phase. During the nucleation process, the two phases still maintain cooperative growth. The initial phase field value of austenite is 1, the first precipitation phase is 0. In this paper, only the first model (the first precipitate is ferrite) was studied since the nucleation principle is basically the same.
The simulation parameters are referenced in the existing literature [10]. Where α denotes ferrite, β denotes cementite, and γ denotes austenite.

Table 1.
Simulation parameters

Parameters	Symbol	Value
Interface energy	$\sigma_{\alpha\beta}$, $\sigma_{\alpha\gamma}$, $\sigma_{\beta\gamma}$	1.0J·m^{-2}
Mobility	α/β $\mu_{\alpha\beta}/\mu_{\beta\alpha}$	9.0×10^{-16}~5.0×10^{-15} m^4·J^{-1}·s^{-1}
	γ/β $\mu_{\gamma\beta}/\mu_{\beta\gamma}$	9.0×10^{-13}~2.0×10^{-12} m^4·J^{-1}s^{-1}
	γ/α $\mu_{\gamma\alpha}/\mu_{\alpha\gamma}$	5.0×10^{-13}~1.0×10^{-12} m^4·J^{-1}s^{-1}
Diffusion coefficient	α $D_{\alpha}=D_{a0}$*exp(-Q_a/RT)	$D_{a0}=2.2\times10^{-4}$ m^2·s^{-1} $Q_a=122.5\times10^3$ J·mol^{-1}
	β D_{β}	Stoichiometry
	γ $D_{\gamma}=D_{\gamma0}$*exp(-Q_{γ}/RT)	$D_{r0}=1.5\times10^{-5}$ m^2·s^{-1} $Q_r=142.1\times10^3$ J·mol^{-1}

4. Results and discussion

The merits and demerits of the different modification methods for nucleation model are discussed. Here, a 200 × 200 grid is set up for the nucleation simulation. The initial phase field distribution is shown in Fig. 2. The initial nucleation position is set to the center of the whole region. The critical nucleation concentrations of the two phases (ferrite and cementite) were 3.2% (mole) and 3.72% (mole), respectively. The calculation method is given below.
As the eutectoid nucleation process is rarely studied, the nucleation critical concentration can only be used for reference to the existing eutectic nucleation. The eutectic nucleation conditions are introduced by Zhu et al. [11], the value of $C_i - C_E$ is greater than or less than a certain value determines whether it is nucleated (C_i is the nucleation concentration mentioned in this article, C_E is the eutectic composition), The value varies with the simulated alloy, 0.8 and -1.8 for the Al-Si alloy [12], 1.6 and -2.5 for the aluminum-magnesium alloy [13] and 1.8 for the CBr_4-C_2Cl_6 [11]. The calculation method of these values is not given in the literature, and there is no solution to deal with the problem correctly. And the solid-phase diffusion coefficient of eutectoid transformation is a small value, the change of concentration is

small, and there is no such a large fluctuation in the liquid phase. Therefore, the nucleation conditions are modified according to the eutectoid transition characteristics. Such as equation (1), $k_{Revision}$ is the correction factor, $C_i^{A,j}$ is the eutectic transformation critical concentration of phase j of alloy A, C_E^A is the eutectic composition of alloy A, C_E^B is the eutectoid composition of alloy B, $C_i^{B,j}$ is the eutectoid transformation critical concentration of j phase of alloy A. Here CBr_4-C_2Cl_6 studied by Zhu et al [11] is used as alloy A, so the relevant parameters can be obtained, $C_i^A - C_E^A$ = 1.8 wt%, C_E^A = 8.4 wt%, C_E^B = 3.46 mol%, $k_{Revision}$=1/3 then the value of $C_i^{B,F}$ is about equal to 3.2 mol%. Unlike ferrite, cementite is a stoichiometric state. The concentration difference of cementite is assumed to be same with the value of ferrite, so $C_i^{B,Cem}$ = 3.72 mol%.

$$C_i^{B,j} = C_E^B + k_{\text{Revision}} \cdot \left(C_i^{A,j} - C_E^A\right) / C_E^A \cdot C_E^B \tag{6}$$

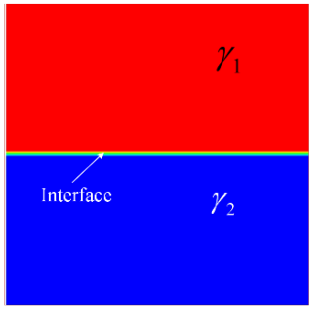

Fig. 2. The distribution of initial phase field

4.1. The results of nucleation simulation without model modification

When the model is not modified, the morphology of nucleation growth is shown in Fig. 3. The growth pattern of the single phase is elliptical, as shown in the ferrite phase of Fig a). When the other phase (in this case, the cementite) cling to the primary-precipitated phase for nucleation, the growth of the two phases in the vertical direction of the austenite grain boundaries satisfies the cooperative growth condition. And a transformation between the two phases occurred in the parallel to the austenite grain boundary. The growth of the cementite (the highest carbon concentration) is bent upward. The reason is that the lamellar thickness of ferrite (the lowest carbon concentration) is too small, the precipitated carbon atoms from the transformation of austenite to ferrite cannot satisfies the captured carbon atoms from the transformation of austenite to cementite when the two phases are cooperation growth, so it needs more austenite to precipitate carbon atoms, that is, ferrite lamellae requires a greater transformation area, the above pattern will formed when the adjustment of ferrite and cementite two-phase is made. In the figure, the difference between the lamellar spacing and the actual lamellar spacing is large, and the nucleation speed is slow, the nucleation model needs to be modified. In order to facilitate comparison, the nucleation law of the unmodified nucleation model is given below.

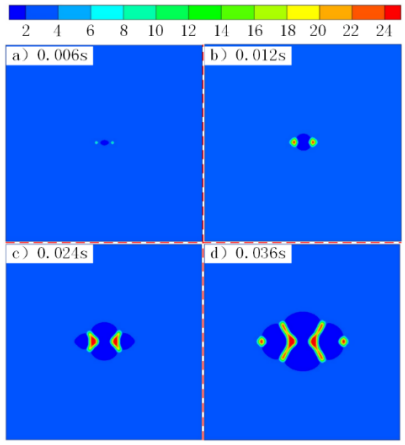

Fig. 3. The morphology of nucleation growth without model modification

4.2. The results of nucleation simulation with modified model

There are four model correction methods:

(1) The interfacial diffusion coefficient is 20 times of the intragranular diffusion coefficient.
(2) The boundary diffusion coefficient is introduced in the boundary region, which is 20 times of the bulk diffusion coefficient.
(3) The introduction of boundary diffusion and the interfacial mobility is 10 times of the intragranular mobility.
(4) The introduction of boundary diffusion and the velocity term is introduced into the grain boundary, Set C_v=2p=2.5e8.

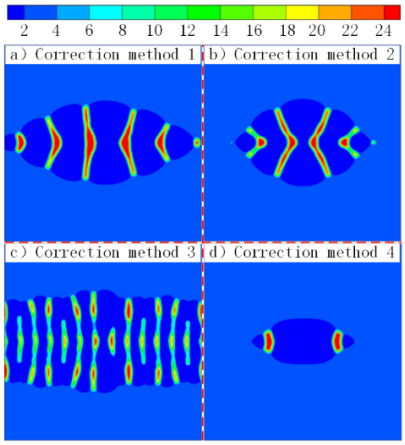

Fig. 4. Concentration distribution of different correction models at 0.048s

Fig. 4 is the concentration distribution of the four nucleation model correction methods at 0.048s, and it reflected the phase distribution at some extent. It can be seen from the figure that the former three models can accelerate the nucleation rate to a certain

extent. The fourth model, although only two cementite nucleus are generated in 0.048s, but the lamellar spacing is larger, closer to the steady-state lamellar spacing. The nucleation rate of the third model is very fast, and the austenite grain boundary were completely occupied by the lamellar nucleus before 0.048s. However, since there are many nucleus, the lamellar spacing is very small, the lamellar merging and annihilation occurs in the subsequent lamellar growth. In order to analyze the regularity for the correction method of nucleation model, the distance-time-phase diagram is drawn for these modified models, as shown in Fig. 5. The correction method 1 is faster than the original nucleation, and the lamellar spacing is large. The correction method 2 is slightly faster than the original nucleation, but the lamellar spacing is slightly smaller; the nucleation of the correction method 3 is very fast and the lamellar spacing is the smallest; the nucleation of the correction method 4 is the slowest, the lamellar spacing is the largest, but also the closest to the steady-state lamellar spacing.

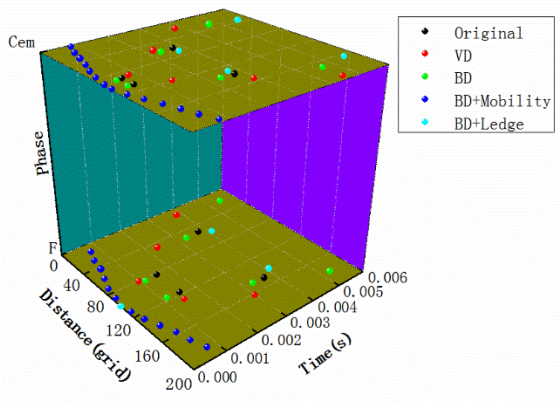

Fig. 5. Distance-time-phase diagram of nucleation with different correction methods (Original is unmodified model, VD is modified model 1, BD is modified model 2, BD+Mobility is modified model 3, BD+Ledge is modified model 4)

In order to quantitatively analyze the nucleation laws of the four models, the concept of nucleation rate V_{Nuc} is proposed. As shown in equation (11), the optimal model is determined by combining the nucleation rate with the nucleation position.

$$V_{Nuc} = \frac{\Delta S}{\Delta t} \tag{11}$$

Where ΔS is the distance between the nucleation sites of the different neighbor phases, Δt is the time different between the nucleuses of different neighbor phases.

According to the above formula, the nucleation site and nucleation rate graph are obtained, as shown in Fig. 6 and Fig. 7. The grid spacing between the two phases shown in Fig. 6 is the nucleation spacing. The ferrite phase with the grid position of 100 is set as the origin, the distance between the first cementite and the preceding ferrite nucleus in different models have following relationship.

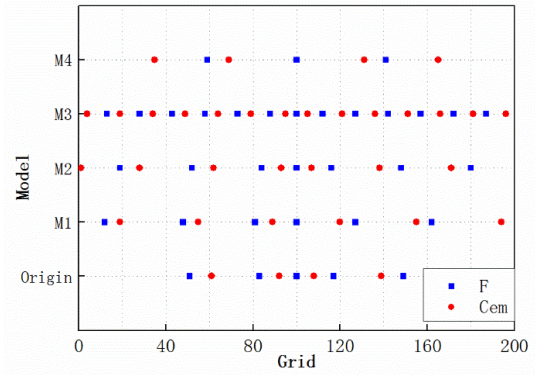

Fig. 6. Comparison of nucleation position of different models

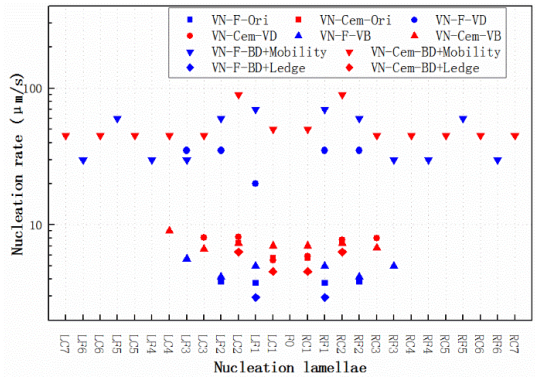

Fig. 7. Comparison of nucleation rate of different models

$$S^0_{F\to Cem,3} < S^0_{F\to Cem,2} < S^0_{F\to Cem,0} < S^0_{F\to Cem,1} < S^0_{F\to Cem,4} \tag{12}$$

By statistical analysis of the subsequent nucleation spacing, the relationship between the average nucleation spacing from ferrite to cementite and the average nucleation spacing from cementite to ferrite can be obtained.

$$S^m_{F\to Cem,3} < S^m_{F\to Cem,0} < S^m_{F\to Cem,2} < S^m_{F\to Cem,4} < S^m_{F\to Cem,1} \tag{13}$$

$$S^m_{Cem\to F,3} < S^m_{\mathrm{Cem}\to F,1} < S^m_{Cem\to F,2} \le S^m_{Cem\to F,0} < S^m_{Cem\to F,4} \tag{14}$$

As the nucleation spacing from cementite to ferrite is small, the corresponding values of the five different models differ little. So the average nucleation spacing from ferrite to cementite was used as a criterion to judge the pros and cons of the model.

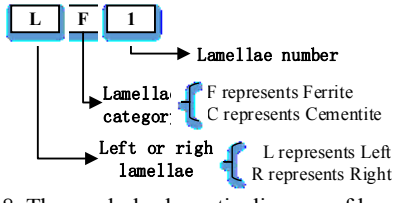

Fig. 8. The symbol schematic diagram of lamellae

Fig. 7 shows the nucleation rate V_{Nuc} of the ferrite or cementite phase. The x-axis corresponds to nucleation lamellae, F0 is the initial ferrite lamellae, the other symbol meaning as shown in Fig. 8. The ferrite phase with the grid position of 100 is set as the origin, the nucleation rate between the first cementite and the preceding ferrite nucleus in different models have following relationship.

$$V^0_{F\to Cem,4} < V^0_{F\to Cem,1} < V^0_{F\to Cem,0} < V^0_{F\to Cem,2} < V^0_{F\to Cem,3} \tag{15}$$

By statistical analysis of the subsequent nucleation rate, the relationship between the nucleation rate from ferrite to cementite and the nucleation rate from cementite to ferrite can be obtained.

$$V^m_{F\to Cem,4} < V^m_{F\to Cem,2} < V^m_{F\to Cem,0} < V^m_{F\to Cem,1} < V^m_{F\to Cem,3} \tag{16}$$

$$V^0_{Cem\to F,4} < V^0_{Cem\to F,0} < V^0_{Cem\to F,2} < V^0_{Cem\to F,1} < V^0_{Cem\to F,3} \tag{17}$$

The relationship between nucleation spacing and nucleation rate of five models was compared.

The correction model 4 and the correction model 3 show two extremes in the nucleation spacing and nucleation rate. Correction mode 4 has the largest nucleus spacing, but the nucleation rate is the smallest. The nucleus spacing of the correction model 3 is the smallest, but the nucleation rate is the largest. The correction model 1 is in the front position in both criteria, so it is more suitable. However, the volume diffusion coefficient at the interface does not conform to the actual theoretical data at this stage. This is why this paper does not discuss the VD + Mobility and VD + Ledge model. Correction model 2 increases the boundary diffusion, although the nucleus position and nucleation speed did not change significantly, but more in line with the actual growth state. Therefore, we need to choose model 3 or model 4 under the condition of introducing boundary diffusion. Model 3 and model 4, to a certain extent, can be equivalent. In principle, they are all to speed up growth of the nucleus at the austenitic boundary. Model 3 increases the nucleation rate by increasing the increment of the phase field in a single time step, while model 4 adjusts the diffusion flux in different directions to increase the concentration increment in a certain direction and accelerate nucleation.

The width of the lamellar ferrite phase occupies about 65% of the lamellar spacing, so the nucleus spacing and nucleation rate of the model should be mainly to promote the formation of ferrite phase. The above model rule is obtained at a determined critical concentration. The nucleation critical concentration of cementite is directly proportional to the nucleus spacing of F → Cem, and is inversely proportional to the nucleation rate of F → Cem. Therefore, if the model 3 is chosen, the nucleation critical concentration of the cementite can be increased appropriately, thereby increasing the nucleus spacing. If the model 4 is chosen, there are two ways to increase the nucleation rate. One way is to increase the mobility by learning from the model 3; the other way is to adjust the velocity control term, and then accelerate the growth rate, but this method cannot significantly increase the nucleation rate. The model 3 and the model 4 are adjusted according to the above-mentioned way.

When the two adjustment models in Fig. 9 are analyzed, it can be seen that the nucleation spacing of model 3 is obviously increased and the nucleation rate of model 4 is greatly enhanced. The initial lamellar ferrite width in model 4 is significantly larger than that in subsequent lamellae, which is approximately twice the width of the subsequent lamellae. That mainly due to the introduction of the velocity term, the initial lamellar ferrite grows in two directions. But the subsequent lamellar ferrite is grown in a single direction cling to the cementite lamellae, so the initial lamellar ferrite growth distance is twice the subsequent lamellar ferrite growth distance at the same time. In order to quantitatively analyze the advantages and disadvantages of the nucleation model, we obtain the nucleation site and nucleation rate of Fig. 10.

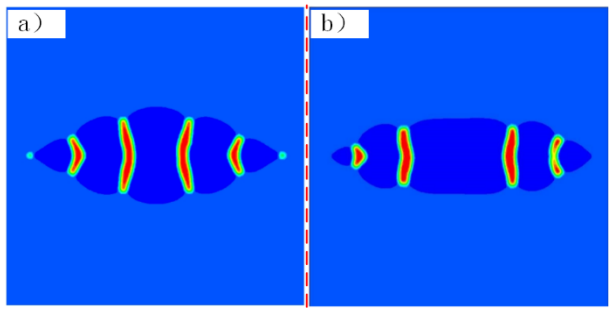

Fig. 9. The morphology of model 3 and model 4 after adjustment at 0.048s. a) the critical concentration of model 3 is 3.80%, b) The boundary mobility of model 4 increased to 3.0 times

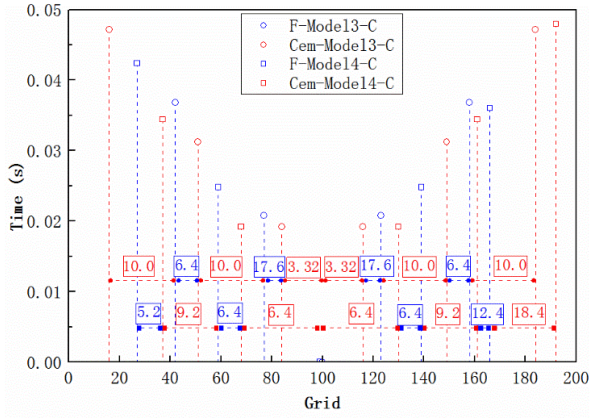

Fig. 10. The nucleation position and nucleation rate (μm·s^{-1}) of model 3 and model 4 after adjusting the parameters

Different symbols in the figure indicate different models, and different colors indicate different phases. The initial cementite nucleation rate of model 3 is 3.32μm·s^{-1}, which is approximately half of the nucleation rate of model 4, and the nucleus spacing is smaller than that of model 4 too, so the model 4 is more practical. Analysis of the subsequent nucleation, the nucleation spacing of model 3 is slightly larger than that of model 4, and the nucleation rate of cementite is relatively stable, which is 10.0μm·s^{-1}, which is slightly larger than that of model 4. The reason for the instability of model 4 is that the initial nucleus is slightly off-center, resulting in different distances from the boundary. In the

comprehensive analysis, model 4 is more suitable for nucleation simulation, and model 4 can control the spacing between nucleuses through velocity term, which is more favorable for nucleation study.

The nucleation process of eutectoid steel is difficult to obtain experimentally, most of the nucleation morphology comes from hypoeutectoid steel or hypereutectoid steel, but the austenite boundary of eutectoid steel often exists pro-eutectoid phase, Ferrite or pro-eutectoid cementite. It is difference from the nucleation hypothesis here. Liu Zongchang et al [14] believe that pearlite nucleus is composed of lamellar ferrite and lamellar cementite. Although the nucleation mechanism is different, the pearlite morphology of simulation is comparable to the actual one. Since the orientation relationship is not considered in this paper, the simulation results show that the pearlite grows to both sides of the austenite at the same time.

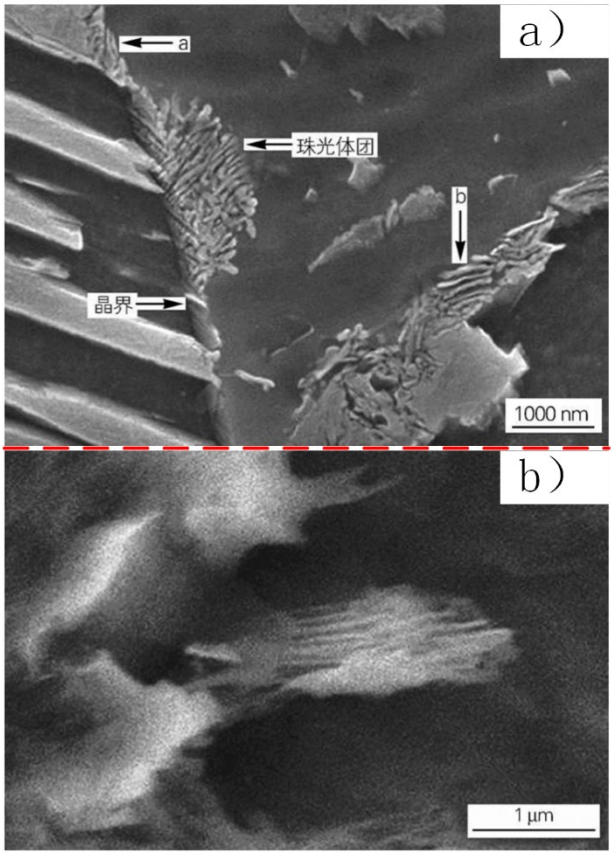

Fig. 11. The process of nucleation and growth for a) 35GrMo steel and b) T8 steel

Fig. 11 [14] shows the morphology of pearlite nucleation growth, the nucleus of pearlite clusters is generally at austenite grain boundaries. In the initial stage, the pearlite clusters grow outwards in semi-elliptical. There is a main direction of lamellar growth, but it is also mixed with other directions or bending growth. This is due to the process of nucleation and growth occur simultaneously. Here, we can only qualitatively compare it with the simulation results. But the growth spacing is an important index of the quantitative pearlite, the spacing between the experiment and simulation is in good agreement with each other. In the simulation, there are 5 pieces of lamellar spacing in the 800nm region, there are six pieces of lamellar spacing in the 1000nm length.

5. Conclusion

Based on the existing nucleation theory, this paper proposes a cooperative nucleation model to simulate the nucleation process of eutectoid growth. A more appropriate nucleation model is obtained by multiple model modifications. And the simulation results are in agreement with the experimental results. The numerical simulation results show that

1. When the model is not modified, the lateral growth of single phase is faster than that of longitudinal growth, so the morphology is oval.
2. The introduction of boundary diffusion in the boundary region is helpful to the nucleation process. Although increasing the coefficient of volume diffusion in the boundary region can get better results, the increase of the volume diffusion coefficient is not consistent with the existing research. But the introduction of boundary diffusion can obtain similar results.
3. When the boundary region is introduced into the boundary diffusion, the introduction of velocity control and boundary mobility can greatly increase the nucleation rate and nucleation spacing.

Acknowledgements

This research was financially supported by National Science & Technology Key Projects of Numerical Control (2012ZX04012-011) and National Natural Science Foundation of China (Grant No. 51305149).

References

[1] Su, Y.Q, Li, X.Z., Guo, J. J. et al. (2006). Phase-field research of microstructure evolution for directionally solidified peritectic transition. Simulation of Nucleation-Controlled Microstructure. *Acta Metallurgica Sinica*. (06), 606-610.

[2] Wu, M.W. & Xiong, S.M. (2011). Modeling of regular eutectic growth of binary alloy based on cellular automaton method. *Acta Phys. Sin-Ch Ed*. 60(5), 757-765.

[3] Liu, Z., Yuan, C., Ji, Y. et al. (2011). Study on nucleation of bainite ferrite. *Transactions of Materials and Heat Treatment*. 32(10), 74-79. DOI:10.13289/j.issn.1009-6264.2011.10.027.

[4] Wang, Y.B., Wang, Y.X. & Chen, Z. et al. (2012). Phase-field Simulation of Interface Effect during Grain Nucleation of Solidification Processing. *Rare Metal Materials and Engineering*. (06), 1045-1048.

[5] Vaks, V.G., Stroev, A.Y. & Urtsev, V.N. et al. (2011). Experimental and theoretical study of the formation and growth of pearlite colonies in eutectoid steels. *J. Exp. Theor. Phys.* 112(6),961-978. DOI:10.1134/S1063776111050098.
[6] Cheng, L. (2013). *The nucleation, three dimensional morphology and growth kinetics of ferrite in low carbon high strength micro-alloyed steels*. Wuhan: University of Science and Technology.
[7] Steinbach, I. & Apel, M. (2006). Multi phase field model for solid state transformation with elastic strain. *Physica D: Nonlinear Phenomena*. 217(2), 153-160. DOI:10.1016/j.physd.2006.04.001.
[8] Steinbach, I., & Apel, M. (2007). The influence of lattice strain on pearlite formation in Fe–C. *Acta Mater.* 55(14), 4817-4822. DOI:10.1016/j.actamat.2007.05.013.
[9] Bottger, B., Eiken, J. & Steinbach, I. (2006). Phase field simulation of equiaxed solidification in technical alloys. *Acta Materialia*. 54(10), 2697-2704. DOI:10.1016/j.actamat.2006.02.008.
[10] Nakajima, K., Apel, M. & Steinbach, I. (2006). The role of carbon diffusion in ferrite on the kinetics of cooperative growth of pearlite: A multi-phase field study. *Acta Mater.* 54(14), 3665-3672. DOI:10.1016/j.actamat.2006.03.050.
[11] Zhu, M.F. & Hong, C.P. (2002). Modeling of microstructure evolution in regular eutectic growth. *Physical Review B*. 66, 155428-1-155428-8. DOI:10.1103/PhysRevB.66.155428.
[12] Chen, R., Xu, Q. & Liu, B. (2016). Modeling of aluminum-silicon irregular eutectic growth by cellular automaton model. *China Foundry*. 13(2), 114-122. DOI:10.1007/s41230-016-5127-6.
[13] Xiong, S.M., Wu, M.W. (2012). Experimental and Modeling Studies of the Lamellar Eutectic Growth of Mg-Al Alloy. 43(1), 208-218. DOI:10.1007/s11661-011-0831-8
[14] Liu, Z.C., Yuan, C.J., Ji, Y.P. et al. (2011). Nucleation of pearlite transformation. *Heat Treatment of Metals*. 36(2),14-17.